Heliyon 10 (2024) e37768

Contents lists available at ScienceDirect

Heliyon

journal homepage: www.cell.com/heliyon

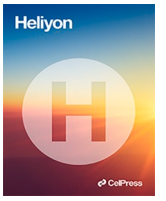

Research article

Adsorption of cadmium from wastewater with activated carbons derived from pig fur biowaste: A comparative study of *in-situ* and *ex-situ* activation routes

Henry Oghenero Orugba [a], Jude Ebieladoh Sinebe [b], Jeremiah Lekwuwa Chukwuneke [c,*], Victor Ikenna Okoro [d], Chukwudi Louis Enyi [b], Okwuchukwu Innocent Ani [e]

[a] *Department of Chemical Engineering, Delta State University, Abraka, Nigeria*
[b] *Department of Mechanical Engineering, Delta State University, Abraka, Nigeria*
[c] *Department of Mechanical Engineering, Nnamdi Azikiwe University, Awka, Nigeria*
[d] *Department of Mechanical Engineering, Imo State University, Owerri, Nigeria*
[e] *Department of Mechanical Engineering, Enugu State University of Science & Technology, Enugu, Nigeria*

ARTICLE INFO

Keywords:
Activated carbon
Pig Fur
Cadmium
In-situ
Ex-situ
Adsorption

ABSTRACT

The environmental challenges associated with cadmium contamination in wastewater have necessitated the development of high-performing activated carbons (ACs) for effective wastewater treatment. Adsorption capacity depends on both the surface area and the adsorption-active functional groups developed on the adsorbent's surface during activation. Proper manipulation of key process variables using the appropriate activation route produces highly efficient and economically viable ACs. This research investigates the viability of pig fur biowaste as a novel precursor for activated carbons using two distinct activation methods—in-situ and ex-situ. Using a central composite design (CCD) of the Response Surface Methodology (RSM), the study systematically examines the effects of impregnation ratio, carbonization temperature, and carbonization time on the cadmium adsorption capacities of the resulting ACs. The optimal conditions for in-situ activation were found to be 691 °C, 175.11 min, and an impregnation ratio of 1.784 g/g, resulting in a cadmium adsorption capacity of 91.57 %. For ex-situ activation, the optimal conditions were 468.8 °C, 80.81 min, and an impregnation ratio of 2.915 g/g, which achieved a higher cadmium adsorption capacity of 91.21 %. Both types of activated carbons maintained high efficiency after five regeneration cycles, indicating they are suitable for long-term applications requiring repeated regeneration. Although both methods produced ACs with comparable cadmium removal efficiency, the ex-situ activation route proved to be more economically viable due to its lower temperature and shorter processing time. This study demonstrates the potential of pig fur biowaste as a sustainable and underutilized resource for AC production and highlights the ex-situ activation route as the more cost-effective approach for producing high-performance adsorbents.

* Corresponding author.
E-mail address: jl.chukwuneke@unizik.edu.ng (J.L. Chukwuneke).

https://doi.org/10.1016/j.heliyon.2024.e37768
Received 15 June 2024; Received in revised form 27 August 2024; Accepted 9 September 2024
Available online 13 September 2024

1. Introduction

The increased industrialization is responsible for the high rate of discharge of heavy metal-bearing wastewater into the surroundings [1]. The direct discharge of heavy metal-containing wastewater into the environment reduces water quality and creates water scarcity problems [2]. Heavy metals accumulate in the environment and living cells because they are non-degradable, thus posing severe health risks and other ecological challenges [3]. This lethal effect of heavy metals on humans and other living organisms has led to strong restrictions on the concentrations of these pollutants in wastewater. A report by Praveen et al. [4] revealed that close to 14,000 deaths per day are associated with water pollution. Among these heavy metals, cadmium is considered highly toxic to humans due to its cancerous effects. Prior to final disposal, wastewater containing cadmium is usually subjected to treatment techniques like adsorption [5–7], chemical oxidation [8], electrocoagulation [9], chemical precipitation [10], and membrane separation [11] in order to reduce their concentrations to permissible levels. The viability of a heavy metal removal technique is usually ascertained in terms of removal efficiency, environmental impact, and cost [12,13]. In terms of the aforementioned parameters, adsorption using activated carbon produced from different precursors like coal and coke peat is usually preferred over the other techniques for removing heavy metals from water [14]. Producing activated carbon from fossil materials is, however, quite expensive and cannot sustain the increased demand for adsorbents for wastewater treatment. Hence the radical search for more readily available materials like feathers, hair, hoof, and horn that are usually classified as keratin waste.

Keratin, a key structural protein in the epithelial cells of animals [15,16], is produced in large quantities from poultry farms, slaughterhouses, and the leather industry [17]. Chen et al. [18] reported that about 11.82 million metric tons of keratin were produced globally in 2020. This high volume produced, coupled with their slow rate of degradation in the environment, has led to their classification as hazardous wastes by the European Union [19]. Keratin waste pollutes water bodies, causing eutrophication, soil acidification, and loss of biodiversity [18]. Although a good number of waste biomasses have been tested as precursors for the production of adsorbents, not much attention has been given to livestock keratin waste. The molecular chain of keratin contains amino, carboxyl, hydroxyl, and sulfhydryl groups that actively participate in adsorbing heavy metals from water [18,20]. Furthermore, the adsorption performance of activated carbon depends on the parent precursor from which it was fabricated and the route and conditions of activation used [21]. Karri & Sahu [22] observed that carbonization temperature and the dosage of the impregnating agent are key process variables that control the activation process. In the adsorption of Cu^{2+} unto activated carbon fabricated from pine cones, Ofomaja et al. [23] revealed that activation temperature and concentration of NaOH were key parameters controlling the adsorption process. In Pb^{2+} adsorption from wastewater, Momcilovic et al. [24] fabricated activated carbon from pine cones impregnated with H_3PO_4 and obtained a highly mesoporous adsorbent with significant oxygen-functional groups on its surface, showing good sorptive capacity. While varying H_3PO_4 impregnation ratio and activation temperature, Astuti et al. [25] synthesized activated carbon from mangrove propagule for the adsorption of lead (II) ions from wastewater. They obtained activated carbon with new pores, and the surface area was increased from 187.18 m^2/g to 267.45 m^2/g. Arneli et al. [26] developed activated carbon from rice husk at different activating temperatures and impregnation ratios of H_3PO_4 and KOH. Their results revealed that H_3PO_4 is a better activating agent, as it produced the highest adsorption capacity of 1.50 mg/g, while KOH produced activated carbon with an adsorption capacity of 0.375 mg/g. Ziezio et al. [27] synthesized activated carbon from spent coffee and reported that porosity increased with impregnation ratio. He et al. [28] obtained highly porous activated carbon from rice husk using KOH as an activating agent. They also performed surface modification using chitosan as a nitrogen source and obtained enhanced CO_2 adsorption performance, reaching up to 5.83 mmol/g at 273 K and 1 bar. Zakaria et al. [29] revealed that impregnation ratio and activation temperature are key parameters that affect the yield and surface area of activated carbon and consequently its adsorption capacity.

Recent studies have concentrated on optimizing the production of activated carbon from biomass through the application of response surface methodology (RSM). This method facilitates precise adjustment of essential parameters, such as activation temperature, duration, and concentration of activating chemicals, to enhance critical properties like surface area, pore volume, and adsorption capacity. RSM has shown to be effective in systematically refining these parameters, ensuring a high surface area for improved adsorption capacity while maintaining economic viability through a reasonable yield [30]. By modeling complex nonlinear interactions, RSM adeptly captures the intricate processes involved in activation [31]. Additionally, the systematic experimental design inherent in RSM minimizes the number of required trials compared to traditional methods, thereby conserving time and resources [32]. Reis et al. [33] employed the Box-Behnken design to optimize the production of graphitic biochar from Norway spruce bark using KOH for azo dye adsorption. They achieved a high adsorption capacity of 320.5 mg/g and a yield of 42.8 % at a temperature of 700 °C, a time of 60 min, and an impregnation ratio of 2. Dessie et al. [34] optimized activated carbon production from Noug stalk with phosphoric acid, achieving a surface area of 473.45 m^2/g and a 53.78 % yield under optimal conditions of 537.50 °C, 127 min, and a 1.95:1 impregnation ratio. In the production of activated carbon, Tsai et al. [35] used a central composite design to optimize CO_2 activation from Honduras mahogany pod husk. The optimal conditions of 800 °C, 1.5 h, and 300 mL/min CO_2 produced activated carbon with a surface area of 1524 m^2/g and a 41.2 % yield.

Many studies have explored surface area enhancement as a means of improving the adsorption capacity of activated carbons without considering the development of surface functional groups. A highly porous adsorbent does not necessarily translate to high adsorption capacity if adsorption-active functional groups are not well developed on its surface. Considering both surface area enhancement and the development of suitable adsorption-active functional groups in the fabrication of activated carbons, the proper manipulation of key process variables such as activation temperature, time, and concentration of the impregnating chemical can help achieve high-performing activated carbons [36]. While this can be accomplished for some biomasses using *in-situ* activation, the *ex-situ* activation route may be more suitable for others. Pig fur biowaste, which is an understudied biomass, is considered in this research; hence, it is important to investigate a suitable activation route for this biomass. Furthermore, since the thermal activation process is

typically energy-intensive [37], a systematic investigation of the key process variables in both activation routes will not only ensure the production of efficient activated carbons but will also help identify the more economically viable route. This research introduces pig fur biowaste as a novel precursor for the production of activated carbon and explores the effectiveness of both *in-situ* and *ex-situ* activation methods. It systematically examines how variations in impregnation ratio, carbonization temperature, and carbonization time affect the efficiency of cadmium ion removal. Phosphoric acid (H_3PO_4), a benign activation agent, was utilized to increase the surface area and introduce active functional groups for enhanced adsorption performance of the activated carbon [38]. Through this investigation, the study not only demonstrates the potential of pig fur biowaste as an underutilized resource but also identifies the most economically viable activation method. Additionally, it employs advanced multivariate modeling techniques, including Response Surface Methodology (RSM), to optimize process conditions and enhance cadmium removal from wastewater, providing a new framework for developing high-performance, cost-effective adsorbents.

2. Materials and methods

2.1. Materials

The keratin waste used as a precursor for activated carbon in this work is pig fur biowaste. Samples of the precursor were obtained from a local slaughterhouse in Agbor, Nigeria, and were initially washed with warm water to remove faecal deposits and dirt [39]. After washing, the samples were sun-dried for 24 h and then subjected to torrefaction at 110 °C for 24 h in a dryer (DGH-9053; China) to further reduce moisture content. The dried samples were then ground using a local hammer mill and sieved to a particle size range of 0.5 mm–1.0 mm. The activating chemical used was phosphoric acid (85 %, Sigma Aldrich, Germany), and both 0.1 M sodium hydroxide (98 %, Sigma Aldrich, Germany) and 0.1 M hydrochloric acid (98 %, Sigma Aldrich, Germany) were used for pH adjustment. All chemicals, including the distilled water used for dilution, were purchased in analytical grade.

2.2. Experimental design using the RSM central composite design (CCD)

To assess the combined effects of impregnation ratio, carbonization temperature, and carbonization time on cadmium removal efficiency, a Response Surface Methodology (RSM) was employed. The design matrix for the experiments was created using the Central Composite Design (CCD) in Design Expert software (V13, Stat-Ease Inc., USA). The ranges of the three process variables are detailed in Table 1.

RSM utilizes a structured set of experiments to explore the relationship between process variables and responses efficiently. The total number of experimental runs (n) in the RSM model is determined by Equation (1):

$$n = 2r(r-1) + p_0 \tag{1}$$

where r represents the number of independent variables used and p_0 is the center point.

2.3. Acid-impregnation and carbonization: in-situ and ex-situ activation

The pig fur biowaste was divided into two portions to explore different activation routes for optimizing cadmium adsorption. The first portion was subjected to *in-situ* acid impregnation, where the sample was treated with phosphoric acid prior to carbonization. The second portion was subjected to *ex-situ* activation, where the raw biomass was first carbonized before acid impregnation.

For the *in-situ* activation, 20 g of the precursor was soaked in varying volumes of 85 % (w/v) phosphoric acid with a density of 1.71 g/mL based on the procedure outlined in Yorgun & Yildiz [40]. The acid-impregnation step was carried out for 18 h under constant stirring at 85 °C [40], following the experimental design matrix presented in Table 2. After impregnation, the samples were filtered, dried in a dryer (DGH-9053; China) at 110 °C for 6 h, and then carbonized in a muffle furnace (GMP-5093) with limited air supply. The carbonized samples were allowed to cool, washed with hot distilled water to remove excess acid, and then dried again in a dryer (DGH-9053; China) at 110 °C for 6 h. The *in-situ* impregnation ratio ($IR_{in\text{-}situ}$) was calculated using Equation (2).

$$IR_{in-situ} = \frac{mass\ of\ H_3PO_4\ in\ solution}{20\ g\ of\ torrenfied\ pighair} \tag{2}$$

In the *ex-situ* activation process, the precursor samples were carbonized prior to acid treatment. For each sample carbonization, 20 g of

Table 1
Ranges of independent variables.

variables and units	symbol	range	
		high	low
IR (g/g)	X_1	2	4
Carb. temp (°C)	X_2	450	750
Carb. time (min)	X_3	60	180

*IR: impregnation ratio, *Carb. temp: carbonization temperature, *Carb. time: carbonization time.

Table 2
Design matrix for cadmium sorption unto adsorbents.

Order	Independent variables			*In-situ* R (%)	*Ex-situ* R (%)
	X_1: IR (g/g)	X_2: Carb temp (°C)	X_3: Carb. time (min)		
1	2.75	600	120	91.35	95.84
2	2.75	600	120	91.26	95.66
3	2.75	600	120	91.43	95.65
4	2.75	348	120	93.26	90.18
5	1.50	750	60	87.33	90.58
6	2.75	600	120	91.30	95.63
7	2.75	600	19	84.75	95.00
8	2.75	600	221	88.26	94.67
9	2.75	600	120	91.28	95.71
10	4.00	450	180	85.81	91.61
11	4.00	750	60	82.92	97.90
12	4.85	600	120	80.99	92.12
13	1.50	450	180	89.47	96.20
14	2.75	600	120	91.20	95.69
15	2.75	852	120	91.87	90.17
16	4.00	450	60	84.14	90.70
17	4.00	750	180	89.23	89.53
18	1.50	450	60	92.12	88.28
19	1.50	750	180	89.65	89.06
20	0.65	600	120	87.61	89.84

the torrefied sample was subjected to carbonization according to the experimental design in Table 2. Due to the mass reduction associated with carbonization, only 10 g of each carbonized sample was used in the subsequent acid-impregnation step. The volume of acid used for each sample was adjusted to match the impregnation ratio used in the in-situ process. The ex-situ impregnation ratio ($IR_{ex\text{-}situ}$) was calculated similarly to the *in-situ* process, using Equation (3).

$$IR_{ex-situ} = \frac{mass\ of\ H_3PO_4\ in\ solution}{10\ g\ of\ activated\ carbon} \tag{3}$$

2.4. Batch adsorption of cadmium ions from solution

Activated carbon effectively removes cadmium ions through surface complexation, where cadmium ions bind to functional groups on the carbon surface, and ion exchange, where cadmium ions replace other cations. Additionally, electrostatic attraction between Cd^{2+} ions and negatively charged sites on the activated carbon surface further enhances cadmium adsorption [41].

Batch adsorption studies were conducted according to the design matrix in Table 2. In each experiment, 100 mL of model wastewater containing 150 mg/L of cadmium was prepared. Both *in-situ* and *ex-situ* activated carbon adsorbents were used at a dosage of 10 g/L [42]. The mixtures were agitated in an incubator shaker at 100 rpm [43]. The pH was maintained at 6 using a digital pH meter (Hanna 1100), as this pH has been shown to be effective for cadmium adsorption [44]. All the experiments were conducted at room temperature. After a 60-min contact time, each sample was centrifuged at high speed for 10 min and decanted. The cadmium ion concentration left unadsorbed in the collected solution was determined by an atomic absorption spectrophotometer (FS240AA). Each experiment was performed in triplicate, and the average values were reported. The percentage removal of cadmium ions (R%) was calculated using Equation (4).

$$R_{\%} = \left(1 - \frac{C_e}{C_0}\right) \text{x } 100 \tag{4}$$

Where C_0 and C_e represent the initial and final cadmium concentrations (mg/L) in the solution, respectively.

The response (percentage of cadmium removal), denoted by R%, was modeled as a function of three independent variables using the quadratic model described in Equation (5).

$$R_{\%} = \beta_0 + \sum_{i=1}^{r} \beta_i x_i + \sum_{i=1}^{r} \beta_{ii} x_i^2 + \sum_{i=1}^{r} \beta_{ij} x_i x_j + \varepsilon \tag{5}$$

The coefficients β_0, β_i, β_{ii}, and β_{ij} correspond to the constant, linear, quadratic, and interactive effects, respectively. The independent variables are denoted by x_i and x_j, with ε representing the model error. To evaluate the model's adequacy, an analysis of variance (ANOVA) was performed using Design Expert software (V13, Stat-Ease Inc., USA), using the p-value and F-value. This analysis identified the significant factors and interactions impacting cyanide percentage removal, thus enhancing the model's predictive accuracy. A lower p-value combined with a higher F-value indicates a more precise model. Statistically, a model term is highly significant if its p-value is less than 0.01, significant if it is between 0.01 and 0.05, and not significant if it exceeds 0.05.

2.5. Characterization of samples

Different characterization techniques were employed in characterizing the raw precursor and the samples that produced the highest percentage of cadmium removal. The characterizations carried out include proximate and ultimate analyses, functional groups, and surface morphology. In order to study the different active functional groups for cadmium adsorption, Fourier transform infrared spectroscopy (FTIR) was performed using the FTIR analyzer (Thermo Fisher Scientific) [45], while the scanning electron microscope (SEM) analyzer (Shimadzu SSX550) was employed in studying the sample microstructures.

2.6. Regeneration and disposal of spent activated carbons

Before final disposal, the activated carbons obtained under optimal conditions from both the *in-situ* and *ex-situ* activation processes were subjected to five cycles of adsorption and desorption to assess their reusability using a chemical regeneration method. The spent activated carbon (AC) was weighed into a 250-mL conical flask containing 50 mL of 0.1 M HCl, and the mixture was stirred with a magnetic stirrer for 60 min at 25 °C. The low pH environment created by HCl helps to displace the cadmium ions from the spent AC, allowing for its regeneration and reuse. HCl is a widely available and relatively inexpensive chemical, making it a practical choice for adsorbent regeneration. After 60 min, the regenerated AC was thoroughly rinsed three times with deionized water to effectively remove the desorbed cadmium ions. The efficiencies of adsorption and desorption were calculated using Equation (4) [46] and 6, respectively.

$$Cy_{desp}(\%) = \frac{Cy_{desp}}{Cy_{adsp}} \text{ x } 100 \tag{6}$$

where C_{ydesp} represents the concentration of desorbed cadmium (mg/g), and C_{yadsp} is the concentration of adsorbed cadmium. Each experiment was conducted in triplicate to evaluate the uncertainty of the measurements. The standard error of the mean (SEM) was calculated to provide error bars, which were then presented as the mean ± SEM within a 95 % confidence interval. After five cycles of regeneration, the spent activated carbon (AC) was responsibly disposed of to prevent environmental contamination. It was collected in hazardous waste containers and stabilized by encapsulating it in concrete, following local regulations to ensure environmental protection and safety compliance.

3. Results and discussion

3.1. Characterization results

3.1.1. Ultimate and proximate analysis results of pig Fur biowaste

The results obtained from the proximate and ultimate analyses of the precursor (pig hair biowaste) are presented in Table 3.

The proximate analysis of the precursor reveals a moisture content of 7.97 %, which is advantageous for the carbonization process as it indicates low energy requirements and a shorter processing time. The fixed carbon content of 17.82 % is moderate, indicating that further enhancement is needed to increase porosity and improve adsorption performance. The high volatile matter content (73.10 %) suggests a potential for high surface area development during carbonization, though careful thermal management is required to avoid excessive loss of useful components. The low ash content (1.77 %) is beneficial, as it ensures minimal non-adsorptive impurities in the final product [47]. The ultimate analysis shows a carbon content of 48.31 %, which supports the precursor's potential for effective adsorption due to the carbon's role in forming a porous structure [48]. The high oxygen content (41.77 %) implies that careful control of the activation conditions is needed to manage volatile compound formation [49]. The moderate nitrogen content (4.01 %) suggests potential for developing active adsorption sites during thermal activation. The very low sulfur content (0.08 %) is favorable for minimizing SO_2 emissions during the activation process, thereby reducing environmental impact [50].

3.1.2. Fourier transform infrared spectroscopy (FTIR) of the precursor and the adsorbents

Fig. 1a–c presents the FTIR spectra and the associated functional groups of the raw precursor, the *in-situ*-derived activated carbon (AC), and the *ex-situ*-derived activated carbon (AC), respectively.

The FTIR spectrum of the raw precursor (pig fur biowaste) in Fig. 1a reveals a complex mixture of organic compounds with various

Table 3
Proximate and ultimate analyses of precursor.

Proximate analysis (%)				
Moisture content (%)	Fixed carbon (%)		Volatile matter (%)	Ash content (%)
7.97	17.82		73.10	1.77
Ultimate analysis (%)				
Carbon'	Hydrogen	Nitrogen	Sulfur	Oxygen[a]
48.31	5.83	4.01	0.08	41.77

a: calculated.

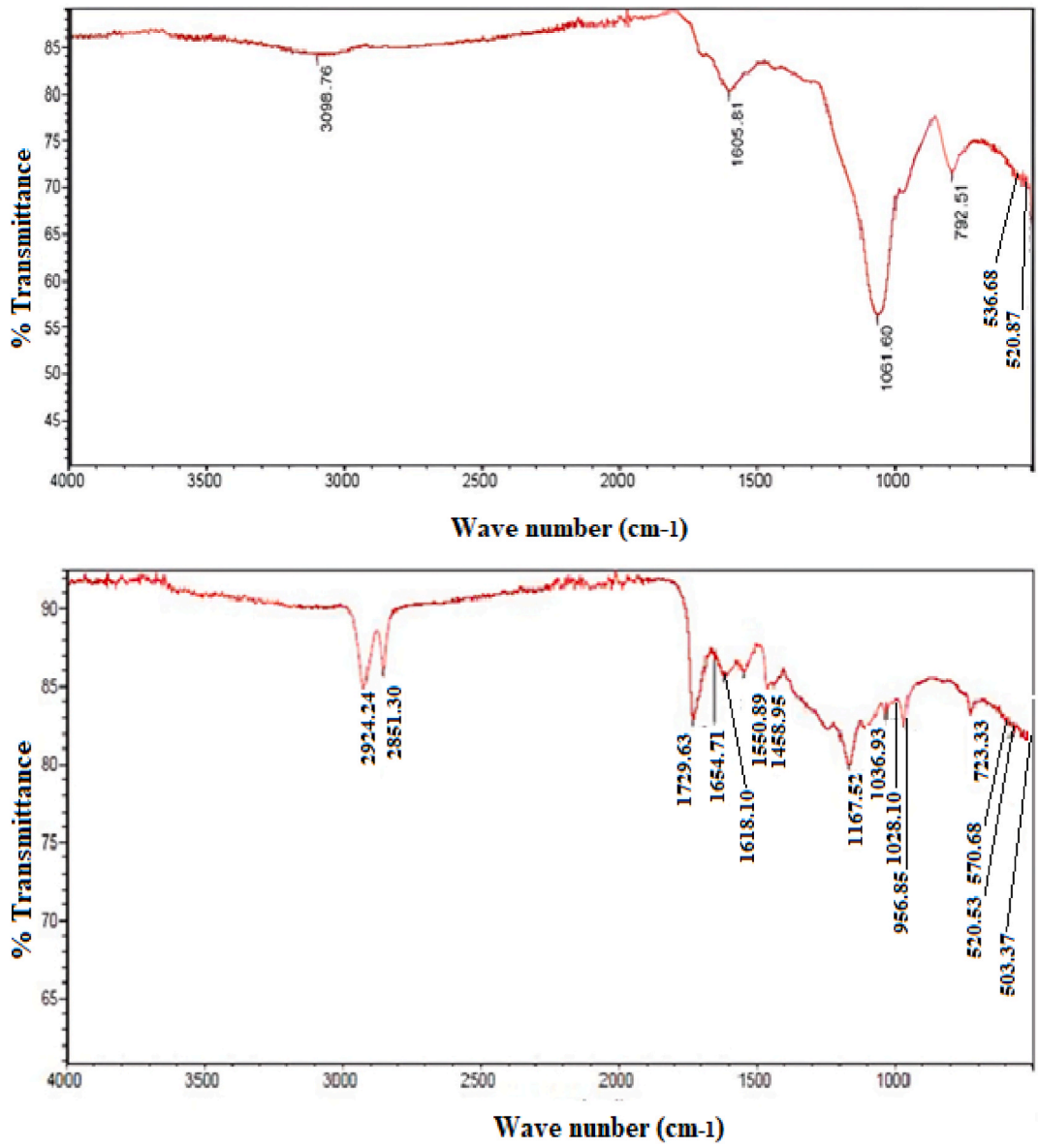

Fig. 1. a: FTIR spectra of the raw precursor
b: FTIR spectra of the in-situ-derived AC
c: FTIR spectra of the ex-situ-derived AC.

functional groups. The peak at 3098.79 cm^{-1} corresponds to the C-H stretching vibration in aliphatic or aromatic groups, indicating the presence of hydrocarbons. The peak at 1605.60 cm^{-1} is attributed to the C=C stretching vibration, suggesting the presence of alkenes and aromatic compounds. The band at 1061.60 cm^{-1} reflects the C-O stretching in ether groups [45], while the peak at 792.51 cm^{-1} is associated with C-H bending in hydrocarbon chains. The peak at 536.68 cm^{-1} corresponds to O-H bending in alcohol groups, indicating the presence of alcohols [20].

The FTIR spectrum of the *in-situ*-derived AC in Fig. 1b shows significant changes compared to the raw precursor, indicating successful chemical activation. Notably, the disappearance of the C=C and C-O groups, which were present in the precursor, suggests the decomposition of lignocelluloses and the volatilization of oxygen-bearing molecules during carbonization [51]. This process breaks down the complex organic matrix, leading to the formation of a more carbon-rich structure. New peaks are observed at 2972.67 cm^{-1} and 2171.49 cm^{-1}, representing C-H stretching in alkanes and C ≡ N stretching in nitriles, respectively. These changes suggest the formation of nitrile groups, which are often introduced during activation processes involving nitrogen-containing reagents or from nitrogen present in the precursor. Peaks at 1570.42 cm^{-1} and 1054.72 cm^{-1} represent N-H bending and C-N stretching of primary

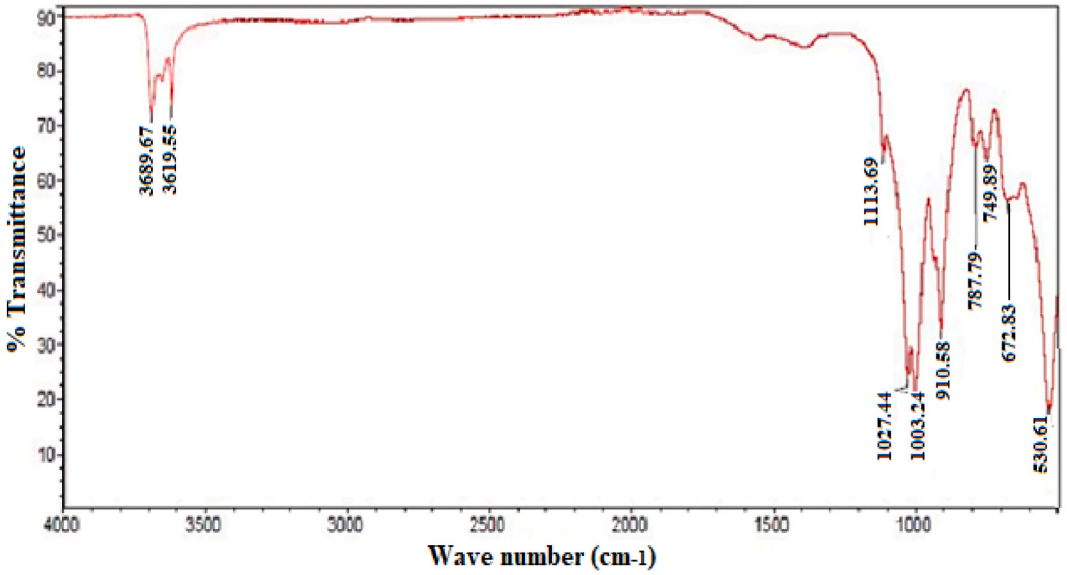

Fig. 1. (*continued*).

amines and amides, respectively, indicating the incorporation of nitrogen functionalities into the activated carbon. The peak at 1013.33 cm^{-1} corresponds to C-H bending vibrations, suggesting the presence of alkanes [20]. The peaks in the range of 574.04 to 510.07 cm^{-1} are associated with C-H out-of-plane bending vibrations specific to aromatic compounds, reflecting the aromatic nature of the carbon structure.

The FTIR spectrum of the *ex-situ*-derived AC in Fig. 1c shows additional changes and the presence of different functional groups compared to the *in-situ*-derived AC. The peak at 3689.67 cm^{-1} is associated with O-H stretching vibrations in alcohols, indicating the presence of hydroxyl groups [38] on the surface of the activated carbon. This can enhance the material's hydrophilicity and adsorption capacity for polar molecules. The peak at 3619.55 cm^{-1} corresponds to N-H stretching vibrations, suggesting the occurrence of secondary amines or amides. This indicates that the ex-situ activation process might introduce different nitrogen-containing functional groups compared to the in-situ process. Peaks at 1113.69 cm^{-1} and 1027.44 cm^{-1} are attributed to C-O stretching and C-N stretching

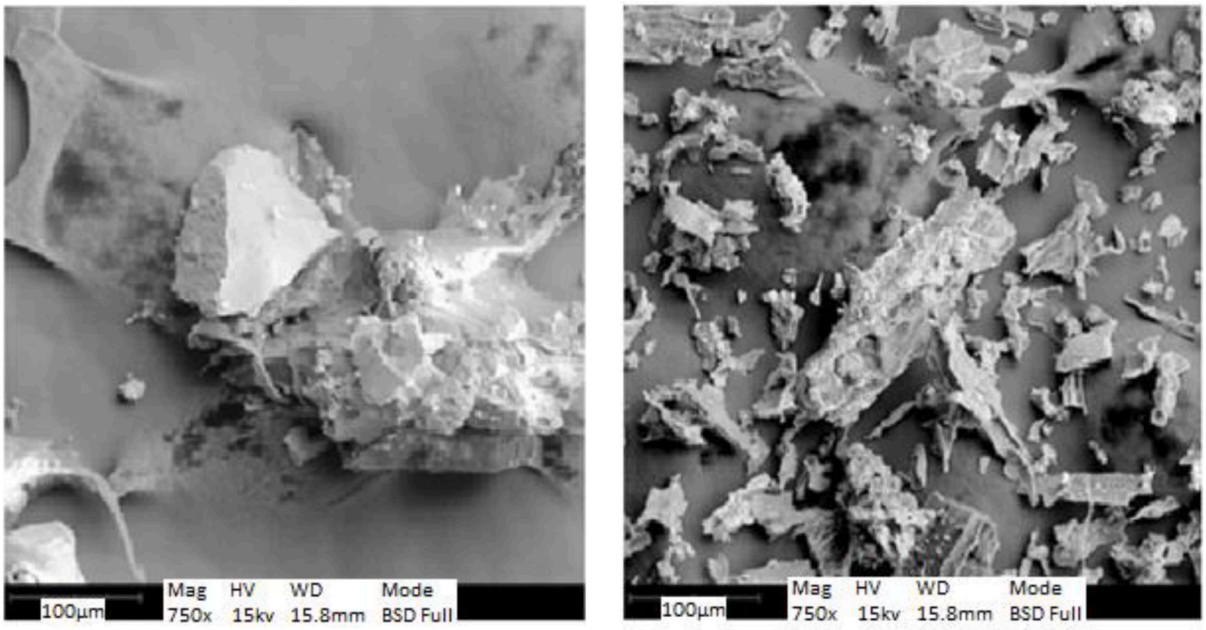

Fig. 2. a: SEM micrograph of the *in-situ*-derived AC
b: SEM micrograph of the *ex-situ*-derived AC.

vibrations, respectively, revealing the occurrence of ethers, esters, and amines. These functional groups can significantly influence the adsorption properties of the activated carbon, particularly for polar or ionic adsorbates. The peaks at 1003.24 cm^{-1}, 910.58 cm^{-1}, 787.79 cm^{-1}, 749.89 cm^{-1}, 672.83 cm^{-1}, and 530.51 cm^{-1} are associated with C-H bending and C-H out-of-plane bending vibrations, characteristic of aromatic compounds [52]. These peaks indicate that the ex-situ-derived AC retains a significant amount of aromatic character, which can contribute to its stability and adsorption capacity for non-polar molecules.

3.1.3. Results of the scanning electron microscopy (SEM) of the activated carbons

The SEM micrographs revealing the morphology of the *in-situ*-derived and *ex-situ*-derived activated carbons (ACs) are presented in Fig. 2a and b, respectively.

The SEM image in Fig. 2a shows the surface morphology of the *in-situ*-derived AC, revealing a highly porous structure typical of activated carbons. These pores, formed by the removal of volatile components during activation [53], create a network of cavities and channels essential for adsorption applications by providing a large surface area for interactions with adsorbate molecules. In contrast, the SEM image in Fig. 2b illustrates the surface morphology of the *ex-situ*-derived AC, which displays a more irregular surface with well-developed pores and a heterogeneous structure compared to the *in-situ*-derived AC. This increased heterogeneity and the presence of irregular-shaped patches suggest a higher degree of activation, likely enhancing the adsorption capacity due to the greater number of active sites [54]. The SEM micrographs confirm significant morphological changes in the precursor due to the activation processes. While the *in-situ*-derived AC has a relatively uniform porous structure, the *ex-situ*-derived AC shows a more complex and heterogeneous surface. These differences are critical for determining the adsorption capacity and efficiency of the activated carbons. The more irregular surface and better-developed pores of the *ex-situ*-derived AC indicate a more effective activation method for creating high-surface-area material with numerous adsorption sites [55]. SEM analysis reveals that both *in-situ* and *ex-situ* activation methods produce highly porous materials essential for adsorption applications. However, the *ex-situ*-derived AC, with its more heterogeneous and irregular surface morphology, demonstrates a higher adsorption capacity.

3.2. Development of in-situ and ex-situ activation models

Using the data in Table 2, the CCD methodology was applied to statistically analyze the combined effects of impregnation ratio (x_1), carbonization temperature (x_2), and carbonization time (x_3) on the percentage of cadmium removal (R%) by the activated carbons from both *in-situ* and *ex-situ* activations. The resulting model equations (based on coded values) for cadmium adsorption onto the activated carbons synthesized via *in-situ* and *ex-situ* activation routes are represented by Equations (7) and (8), respectively.

$$R_{\%in-situ} = 91.30 - 2.02X_1 - 0.3482X_2 + 0.9935X_3 + 0.8521X_1X_2 + 1.04X_1X_3 + 1.20X_2X_3 - 2.47X_1^2 + 0.4476X_2^2 - 1.69X_3^2 \quad (7)$$

$$R_{\%ex-situ} = 95.70 + 0.6919X_1 + 0.0192X_2 - 0.1181X_3 + 1.250X_1X_2 - 1.73X_1X_3 - 2.34X_2X_3 - 1.68X_1^2 - 1.96X_2^2 - 0.3129X_3^2 \quad (8)$$

where $R_{\%in\text{-}situ}$ is the percentage of cadmium removed in the in-situ activated sample, and $R_{\%ex\text{-}situ}$ is the percentage of cadmium removed in the ex-situ activated sample. The variables x_1, x_2, and x_3 represent impregnation ratio, activation temperature, and time, respectively.

In terms of actual factors, the in-situ and ex-situ models are represented by Equations (9) and (10), respectively.

$$R_{\%in-situ} = 105.2413 + 2.70243\,IR - 0.054718\,Temp + 0.011322\,Time + 0.004545\,IR \text{ x } Temp + 0.013851\,IR \text{ x } Time + 0.000134\,Temp \text{ x } Time - 1.58333\,IR^2 + 0.000020\,Temp^2 - 0.000471 Time^2 \quad (9)$$

$$R_{\%ex-situ} = 38.20959 + 5.23908\,IR + 0.11764\,Temp + 0.23849\,Time + 0.006643\,IR \text{ x } Temp - 0.023103\,IR \text{ x } Time - 000260\,Temp \text{ x } Time - 1.0725\,IR^2 - 0.000087\,Temp^2 - 0.000087\,\text{Time}^2 \quad (10)$$

3.3. Analysis of variance (ANOVA) for the Generated models

The adequacy and statistical significance of the cadmium sorption models using in-situ and ex-situ activated carbons were evaluated through an analysis of variance (ANOVA). The ANOVA summary table for these models is presented in Table 4.

The ANOVA results presented in Table 4 reveal that both the *in-situ* and *ex-situ* models are highly significant at a 95 % confidence level, as their p-values are much smaller than 0.05 (<0.0001). This indicates that both models are statistically significant and effectively capture the relationship between the variables influencing cadmium sorption. The comparison of F-values between the two models shows that the *ex-situ* model has a substantially higher F-value (4134.75) compared to the *in-situ* model (1804.15). A higher F-

Table 4
ANOVA summary for cadmium sorption models.

Source	SS	DF	MS	F	P
In-situ model	225.66	9	25.07	1804.15	<0.0001
Ex-situ model	174.34	9	19.37	4134.75	<0.0001

value implies that the *ex-situ* model explains a greater proportion of the variance in the data, indicating it has stronger predictive capability.

Furthermore, the significance of individual model terms was assessed through their p-values and F-values, as presented in Tables 5a and 5b for the in-situ and ex-situ models, respectively. At the 5 % level of significance, terms with p-values less than 0.05 are considered significant contributors to the model [39]. The F-values quantify the impact of each term, with higher values indicating a greater influence on cadmium sorption.

The ANOVA summary table for the cadmium sorption model using the *in-situ* derived adsorbent reveals that all the model terms are highly significant, as indicated by their p-values being less than 0.0001. Among the linear terms, x_1 had the highest influence on cadmium adsorption, with an F-value of 4014.42. For the quadratic terms, x_1^2 exhibited the highest influence with an F-value of 6346.73, while x_2^2 had a lower influence with an F-value of 207.77. Regarding the interaction effects, the x_2x_3 term demonstrated the highest influence on cadmium adsorption capacity with an F-value of 831.57, whereas the x_1x_2 term had the least influence with an F-value of 417.98.

Similarly, the ANOVA summary table for the cadmium sorption model using the *ex-situ* derived activated carbon reveals that, except for x_2, all the model terms are significant, as indicated by their p-values being less than 0.0001. Among the linear terms, x_1 exhibited the highest influence on cadmium adsorption, with an F-value of 1395.58. For the quadratic terms, x_2^2 had the highest influence with an F-value of 11825.19, while x_3^2 had the least influence with an F-value of 301.21. Regarding the interaction effects, the x_2x_3 term demonstrated the highest influence on cadmium adsorption capacity with an F-value of 9358.29, whereas the x_1x_2 term had the least influence with an F-value of 2648.99.

After eliminating the non-significant term (x_2) from the *ex-situ* model, the resultant equation is shown in Equation (11).

$$R_{\%ex-situ} = 95.70 + 0.6919X_1 - 0.1181X_3 + 1.250X_1X_2 - 1.73X_1X_3 - 2.34X_2X_3 - 1.68X_1^2 - 1.96X_2^2 - 0.3129X_3^2 \quad (11)$$

The fitness of each of the models was further ascertained using some statistical indicators, as presented in Table 6.

The performance of the models was assessed using several statistical indicators. The coefficient of determination (R^2) was 0.999 for both in-situ and *ex-situ* models, indicating an excellent fit. The adjusted R^2 values were also 0.999 for both models, signifying a high level of explanatory power while accounting for the number of predictors in the models. The predicted R^2 values were 0.996 for the *in-situ* model and 0.999 for the *ex-situ* model, showing strong predictive capability. The adequate precision, which measures the signal-to-noise ratio, was 146.933 for the in-situ model and 197.727 for the *ex-situ* model. Since a ratio greater than 4 is desirable, these high values indicate that both models are highly reliable and can effectively navigate the design space. The coefficient of variation (CV) was 0.133 % for the *in-situ* model and 0.074 % for the *ex-situ* model. A lower CV indicates that the residuals are small relative to the predicted values, further confirming the models' robustness and reliability. The low CV values obtained suggest that both models are highly precise and accurate in predicting cadmium sorption.

To further evaluate the adequacy of the models for predicting cadmium sorption, the predicted data were plotted against the experimental data, as illustrated in Fig. 3a and b for the adsorbents synthesized via *in-situ* and *ex-situ* activation routes, respectively. The normal probability plots of the residuals that display the percentage probability against the externally studentized residuals for the in-situ and ex-situ models are shown in Fig. 4a and b, respectively.

As shown in Fig. 3a and b, the data points are closely aligned along the diagonal line, which represents a perfect correlation between predicted and actual values. This close alignment indicates a high degree of accuracy in the models' predictions. The high correlation observed in these plots signifies that the models effectively capture the underlying relationship between the variables influencing cadmium sorption for both in-situ and ex-situ-derived activated carbon (AC).

In Fig. 4a and b, the residuals are predominantly located along the straight line, with only minor deviations. This alignment suggests that the residuals are approximately normally distributed, indicating that the models meet the assumption of normality for the residuals. The approximate normal distribution of residuals further validates the models' adequacy in predicting cadmium sorption.

3.4. Optimization of process variables

Figs. 5–7 are the 3D surface plots of the predicted percentage cadmium removal using the adsorbents fabricated via *in-situ* and *ex-situ* activation routes.

Table 5a
Evaluation of the significance of the cadmium sorption model using in-situ-derived AC.

Factor	Coefficient	SS(=MS = DF = 1)	F	P	significance of term
X_1	−2.02	55.79	4014.42	<0.0001	highly significant
X_2	−0.3482	1.66	119.13	<0.0001	highly significant
X_3	0.9935	13.48	969.92	<0.0001	highly significant
X_1X_2	0.8521	5.81	417.98	<0.0001	highly significant
X_1X_3	1.04	8.63	621.24	<0.0001	highly significant
X_2X_3	1.20	11.56	831.57	<0.0001	highly significant
X_1^2	−2.47	88.2	6346.73	<0.0001	highly significant
X_2^2	0.4478	2.89	207.77	<0.0001	highly significant
X_3^2	−1.69	41.39	2978.34	<0.0001	highly significant

Table 5b
Evaluation of significance of cadmium sorption model using ex-situ-derived AC.

Factor	Coefficient	SS(=MS = DF = 1)	F	P	significance of terms
X_1	0.6919	6.54	1395.58	<0.0001	highly significant
X_2	0.0192	0.005	1.08	0.3239	not significant
X_3	−0.1181	0.1905	40.67	<0.0001	highly significant
X_1X_2	1.25	12.41	2648.99	<0.0001	highly significant
X_1X_3	−1.73	24.02	5127.00	<0.0001	highly significant
X_2X_3	−2.34	43.84	9358.29	<0.0001	highly significant
X_1^2	−1.68	40.47	8638.59	<0.0001	highly significant
X_2^2	−1.96	55.4	11825.19	<0.0001	highly significant
X_3^2	−0.3129	1.41	301.21	<0.0001	highly significant

Table 6
Fitness summary of the models.

Test	In-situ model	Ex-situ model
Std. dev	0.118	0.068
Mean	88.76	93.00
C.V. %	0.133	0.074
R^2	0.999	0.999
Adj. R^2	0.999	0.999
Pred. R^2	0.996	0.999
Adeq. Precision	146.933	197.727

3.4.1. Influence of carbonization temperature and impregnation ratio on cadmium adsorption

Fig. 5a and b illustrate the synergistic effects of carbonization temperature and impregnation ratio on the percentage of cadmium removal for *in-situ* and *ex-situ*-derived activated carbons (ACs), respectively.

Both figures (Fig. 5a and b) display a similar trend: cadmium removal efficiency initially increases with rising carbonization temperature and impregnation ratio. This initial increase in cadmium removal can be attributed to the enhanced porosity of the adsorbent, which improves with higher impregnation ratios, as noted by Ziezio et al. [27]. Enhanced porosity increases the available surface area for cadmium adsorption. However, beyond a certain point, further increases in these parameters result in a decline in cadmium removal efficiency.

For the *in-situ*-derived AC (Fig. 5a), the cadmium removal efficiency starts to decrease when the impregnation ratio exceeds 2.5 g/g at higher carbonization temperatures. This reduction can be explained by the transformation of micropores into mesopores, which are less effective for cadmium adsorption. Additionally, higher carbonization temperatures and impregnation ratios can lead to the decomposition of phosphate esters, causing pore structure shrinkage, as reported by Zakaria et al. [29].

In the case of the *ex-situ*-derived AC (Fig. 5b), the decline in cadmium removal efficiency is observed at impregnation ratios above 3.0 g/g and higher carbonization temperatures. This phenomenon could be due to the shielding effect of the impregnating chemical, which occupies the active adsorption sites and hinders cadmium adsorption. Zakaria et al. [29] also observed that excessive use of impregnating chemicals can reduce adsorption efficiency. For example, they achieved a maximum adsorption capacity of 74.7 mg/g at 300 °C and an impregnation ratio of 4. Furthermore, Liou [56] found that temperatures above 500 °C can lead to pore collapse, reducing the surface area and adsorption capacity of the adsorbent. Lam et al. [57] recommended using a moderate concentration of activating chemicals, as excessive amounts can destroy the pore structure during heating. Du et al. [58] suggested an optimal impregnation ratio of 2 at an activation temperature of 600 °C.

3.4.2. Interaction effect of impregnation ratio and carbonization time on cadmium percentage removal

The results presented in Fig. 6a and b demonstrate the influence of impregnation ratio and carbonization time on the cadmium removal efficiency of the *in-situ* and *ex-situ*-derived activated carbons.

For the *in-situ*-derived activated carbon (Fig. 6a), cadmium removal efficiency initially increases from around 80 % to over 90 % as both the impregnation ratio and carbonization time are increased. This is because longer carbonization periods promote the development of surface area and pore volume [40]. Moderate impregnation ratios around 2 g/g also increase porosity [27]. However, prolonged carbonization of the highly impregnated precursor (impregnation ratios above 2.5 g/g and carbonization times over 150 min) increases the rate of phosphate ester decomposition, which shrinks the pore structures and reduces cadmium removal efficiency down to around 85 % [29]. This suggests that for *in-situ*-derived activated carbon, a prolonged carbonization period and higher impregnation ratios can have a negative impact on the adsorption process.

In contrast, for the *ex-situ*-derived activated carbon (Fig. 6b), the cadmium removal efficiency starts at around 90 % and declines to around 85 % as both the impregnation ratio and carbonization time are increased. This decline could be due to the fact that even though numerous micropores were developed on the adsorbent during the prolonged activation of the raw precursor, the high concentration of impregnating chemicals leaves fewer adsorption sites available for cadmium adsorption.

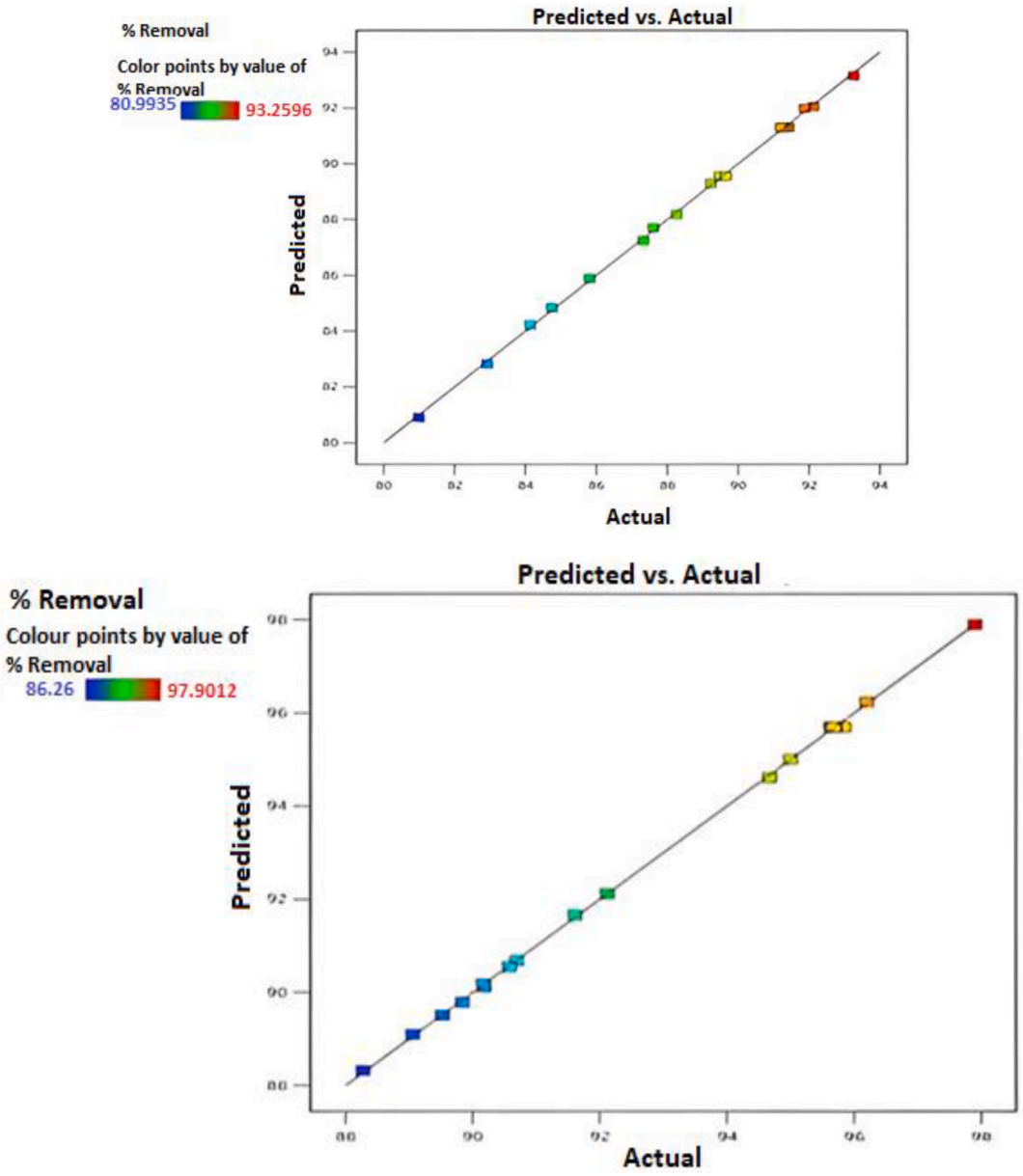

Fig. 3. a: Graph of predicted and actual for cadmium sorption model (*in-situ*-derived AC)
b: Graph of predicted and actual for cadmium sorption model (*ex-situ*–derived AC).

3.4.3. Interaction effect of carbonization temperature and time

The interaction effects of carbonization temperature and time on the percentage cadmium removal using *in-situ* and *ex-situ*-derived activated carbons are depicted in Fig. 7a and b, respectively.

For the *in-situ*-derived activated carbon (Fig. 7a), increasing the carbonization temperature and time gradually increased the percentage of cadmium removal. At lower temperatures around 450 °C and shorter times of 60 min, the cadmium removal was around 80 %. However, as the carbonization temperature was increased to 750 °C and the time extended to 180 min, the cadmium removal percentage continued to rise, reaching over 90 %. This improvement in cadmium adsorption is likely due to the fact that at moderate impregnation ratios, prolonged activation times and elevated temperatures enhance the formation of more micropores on the adsorbents [58] and also develop oxygen-bearing functional groups that improve adsorption [24]. Even at the highest temperatures and longest times tested, the cadmium removal percentage continued to increase, suggesting that further enhancements in porosity and surface chemistry were achieved.

For the *ex-situ*-derived activated carbon (Fig. 7b), the cadmium removal efficiency increases from around 88 % at the lower temperature and time conditions, reaches an optimum of around 92 % at moderate conditions, but then declines to around 85 % as

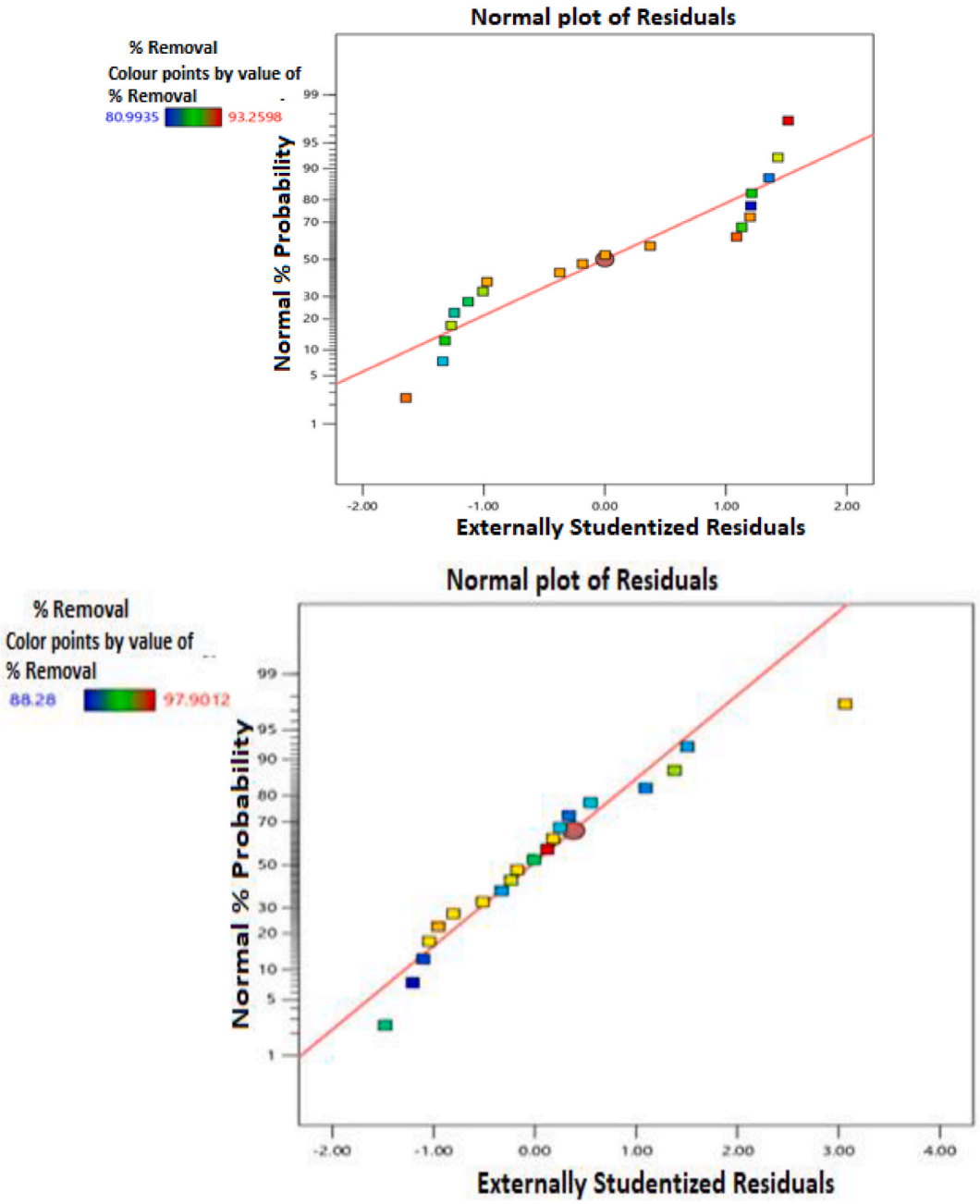

Fig. 4. a: Normal probability curve of residuals for cadmium sorption model (in-situ AC)
b: Normal probability curve of residuals for cadmium sorption model (ex-situ AC).

both the carbonization temperature and time are further increased. This initial increase, followed by a decline in performance, is likely due to the fact that at moderate temperatures and times, numerous micropores are developed on the adsorbent during the activation of the raw precursor. However, as the temperature and time are increased beyond the optimum, the high concentration of impregnating chemicals leaves fewer adsorption sites available for cadmium adsorption [29].

The optimum values obtained from the optimization step were used to perform new sets of experiments in order to validate the models' adequacies, and the results obtained are presented in Table 7.

The results shown in Table 7 demonstrate a high correlation between the experimental and predicted results at the optimum levels, confirming the accuracy of the models. For the *in-situ*-derived activated carbon, the optimum conditions were an impregnation ratio (IR) of 1.784 g/g, a carbonization temperature of 691 °C, and a carbonization time of 175.11 min. At these optimum conditions, the experimental cadmium adsorption percentage was 91.57 %, which is very close to the predicted value of 90.355 %. In contrast, the

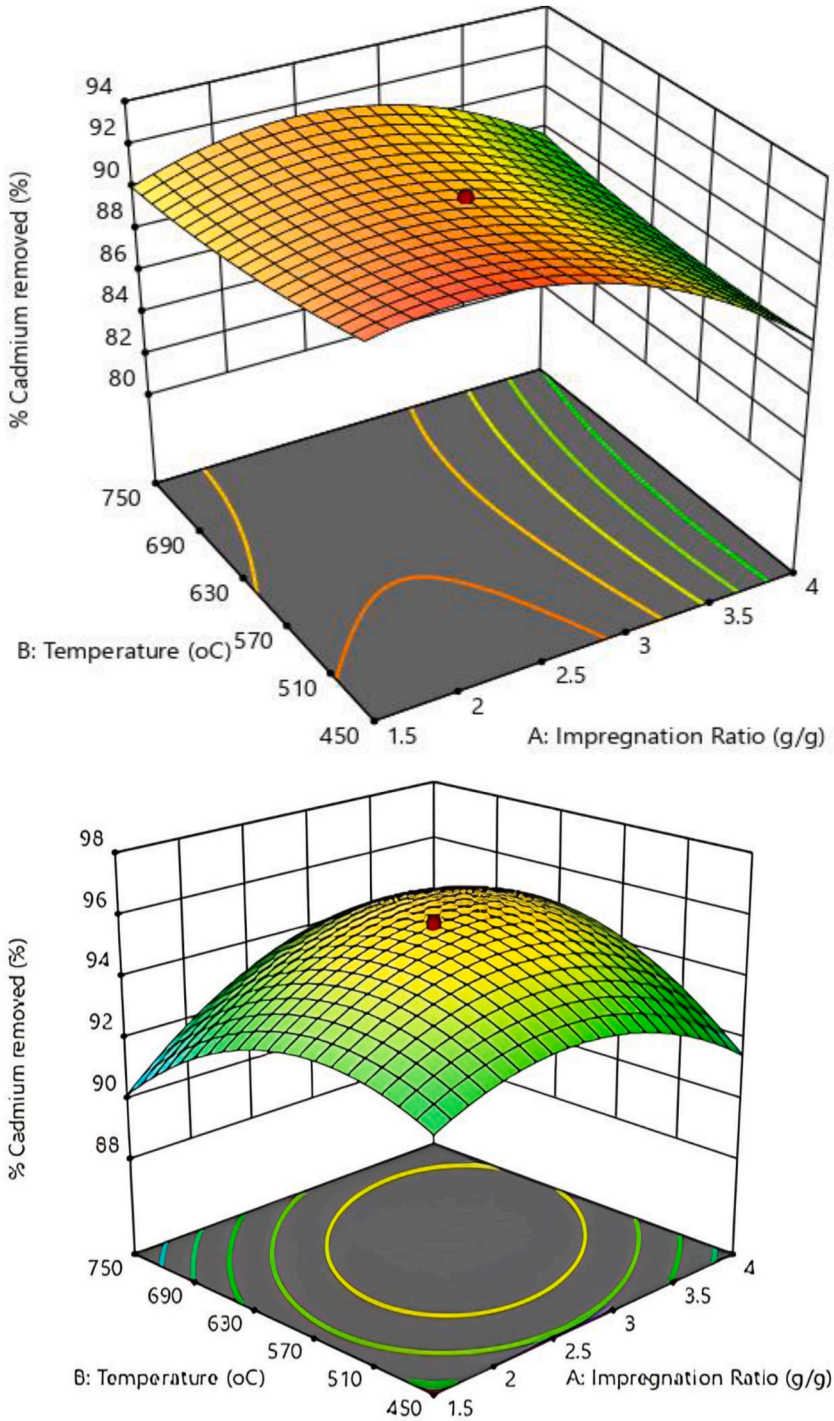

Fig. 5. a: Influence of carbonization temperature and impregnation ratio on percentage cadmium removal using *in-situ*-derived AC (carbonization time at mean value)
b: Influence of carbonization temperature and impregnation ratio on percentage cadmium removal using *ex-situ*-derived AC (carbonization time at mean value).

optimum conditions for the *ex-situ*-derived activated carbon were an impregnation ratio of 2.915 g/g, a carbonization temperature of 468.8 °C, and a carbonization time of 80.81 min. At these conditions, the experimental cadmium adsorption percentage was 91.21 %, which is also very close to the predicted value of 92.85 %. The close agreement between the experimental and predicted values demonstrates the robustness of the models in capturing the complex interactions between the process variables.

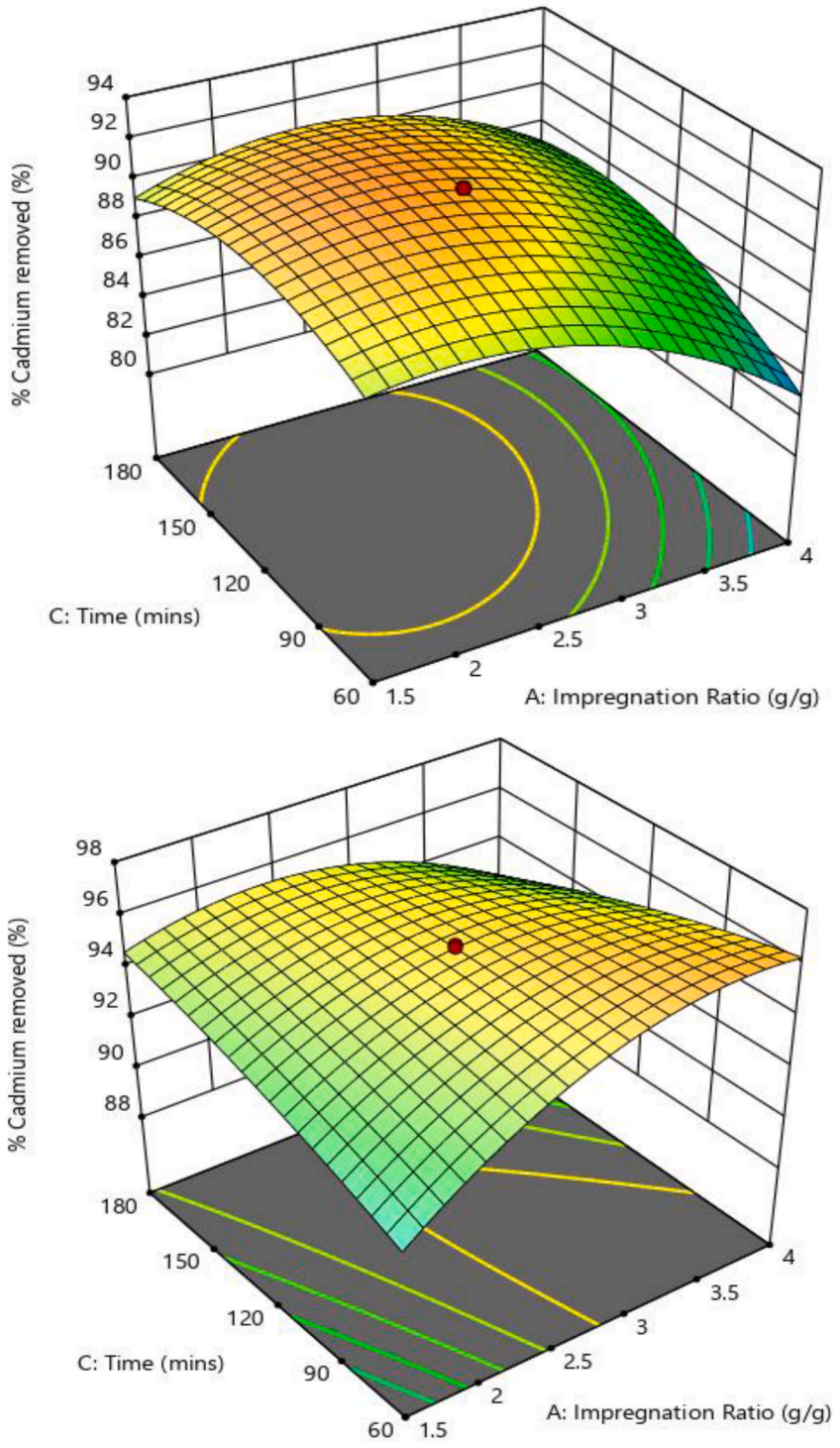

Fig. 6. a: Effect of impregnation ratio and carbonization time on cadmium percentage removal using in-situ derived AC (carbonization temperature at mean value)
b: Effect of impregnation ratio and carbonization time on cadmium percentage removal using ex-situ-derive AC (carbonization temperature at mean value).

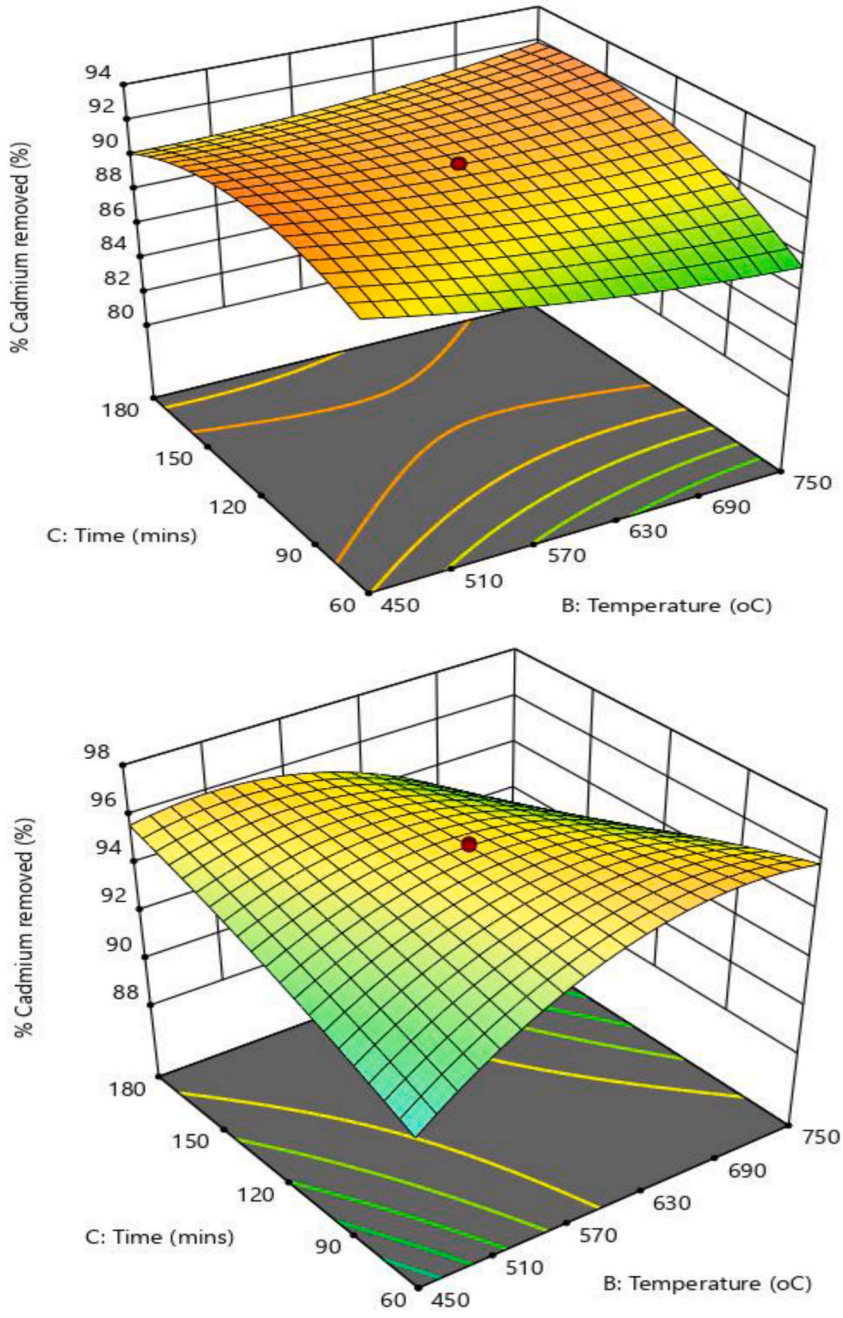

Fig. 7. a: Effect of carbonization temperature and time on percentage cadmium removal using in-situ-derived AC (impregnation ratio at mean value)
b: Effect of carbonization temperature and time on percentage cadmium removal using ex-situ-derived AC (impregnation ratio at mean value).

3.5. Results of regeneration of spent activated carbons

The reusability of the two derived activated carbons was evaluated by conducting five adsorption and desorption cycles. The results are illustrated in Fig. 8a and b for the in-situ and ex-situ derived carbons, respectively.

The data presented in Fig. 8a and b shows that the adsorption efficiency of both *in-situ* and *ex-situ* activated carbons gradually decreases with each successive regeneration cycle. For the *in-situ*-derived activated carbon, the removal efficiency dropped from an initial 92 %–68 % after being reused five times. A similar trend was observed for the *ex-situ*-derived activated carbon, with its efficiency declining from 91 % to 67 % over the same number of cycles. The similar percentage decrease in adsorption efficiency for both

Table 7
Model Validation and Comparison using the Optimum Conditions.

Variable	In-situ			Ex-situ		
	Optimum variable	% cadmium adsorbed		Optimum variable	% cadmium adsorbed	
		Experimental	Predicted		Experimental	Predicted
IR (g/g)	1.784	91.57	90.355	2.915	91.21	92.85
Carb. temp. (°C)	691	–	–	468.8	–	–
Carb. time (min)	175.11	–	–	80.81	–	–

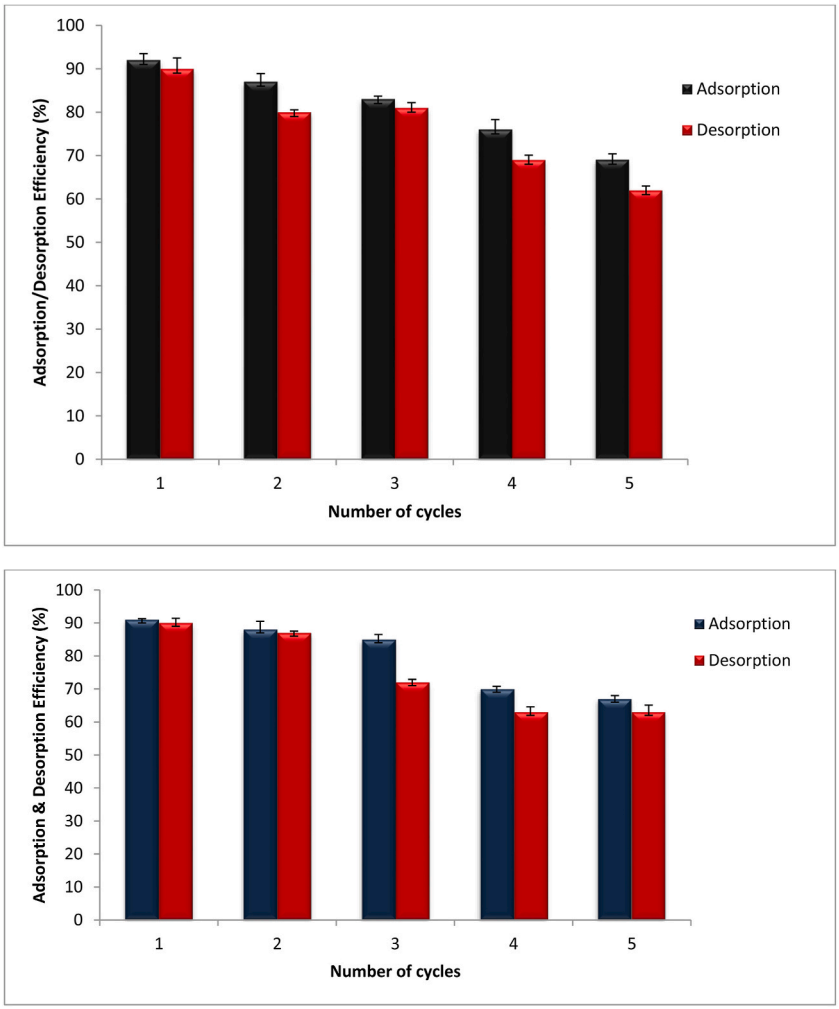

Fig. 8. a: Regeneration efficiency of the *in-situ*-derived AC
b: Regeneration efficiency of the *ex-situ*-derived AC.

activated carbons is likely due to comparable deactivation of active sites, structural changes, and loss of functional groups during regeneration. Despite this gradual reduction in performance, it is noteworthy that both types of activated carbons were still able to maintain relatively high efficiency even after undergoing five regeneration cycles. This finding suggests that these materials have the potential to be utilized for extended periods in applications that necessitate repeated regeneration, as they retain a significant portion of their adsorption capacity even after multiple uses.

3.6. Evaluation of cadmium removal efficiency of the activated carbons

The cadmium removal efficiencies of activated carbons derived from different precursors are presented in Table 8.
As revealed in Table 8, the *in-situ*-derived AC achieved a cadmium removal efficiency of 91.57 %, while the *ex-situ*-derived AC had

Table 8
Comparison of Cadmium Removal Efficiencies of Activated Carbons obtained from different Precursors.

S/No	Precursor used	Cadmium removal (%)	Activating chemical	Reference
1	Pig fur biowaste (*in-situ-derived)*	91.57	H_3PO_4	Present study
2	Pig fur biowaste (*ex-situ-derived)*	91.21	H_3PO_4	Present study
3	*Salvadora perica* stem	81.7	H_2SO_4	[59]
4	Fish scales	88.2	–	[60]
5	*Ziziphus lotus*	60	H_2SO_4	[61]
6	Coffee grounds	50	H_2SO_4	[61]

an efficiency of 91.21 %. These efficiencies are notably higher than those of several other biomass-derived activated carbons. This comparison underscores the strong potential of pig fur biowaste as an effective and sustainable precursor for producing high-performance activated carbons, making it a viable alternative for efficient cadmium removal in wastewater treatment.

4. Conclusion

This research aimed to fabricate high-performance activated carbon (AC) from pig fur biowaste, focusing on enhancing surface area and developing surface functional groups to promote high cadmium removal efficiencies. By optimizing key process variables—impregnation ratio, carbonization temperature, and carbonization time—significant improvements in adsorption capacity were achieved. To determine a more economically viable route, the study tested two activation methods: in-situ and ex-situ. The Response Surface Methodology (RSM) results revealed that both methods produced ACs with substantial cadmium adsorption capacities. Although the two different routes produced comparative cadmium removal efficiency, the ex-situ method appeared to be more economically viable due to its lower activation temperature and time requirement. Furthermore, both types of ACs maintained high efficiency after five regeneration cycles, indicating their suitability for long-term wastewater treatment applications. This study highlights pig fur biowaste as a novel and sustainable precursor for AC production and identifies the ex-situ activation route as the preferred method for achieving high-performance, cost-effective adsorbents with enhanced surface area and active functional groups for superior cadmium removal.

CRediT authorship contribution statement

Henry Oghenero Orugba: Writing – original draft, Validation, Software, Formal analysis, Conceptualization. **Jude Ebieladoh Sinebe:** Validation, Methodology, Investigation, Formal analysis. **Jeremiah Lekwuwa Chukwuneke:** Writing – original draft, Software, Formal analysis, Conceptualization. **Victor Ikenna Okoro:** Software, Resources, Project administration, Investigation, Data curation. **Chukwudi Louis Enyi:** Visualization, Project administration, Methodology, Data curation. **Okwuchukwu Innocent Ani:** Writing – review & editing, Supervision, Resources, Methodology, Investigation.

Declaration of competing interest

The authors declare no conflict of interest.

References

[1] P. Omuku, C. Odidika, A. Ozukwe, K. Iwuozor, A comparative evaluation of rain water obtained from corrugated roofing sheets within Awka Metropolis, Anambra state, Iranical Journal of Energy and Environment 13 (2) (2022) 134–140.
[2] K.O. Iwuozor, T.A. Abdullahi, L.A. Ogunforowa, E.C. Emenike, P.O. Ifeoluwa, F.A. Gbadamosi, J.O. Ighalo, Mitigation of levofloxacin from aqueous media by adsorption: a review, Sustainable Water Resources Management 7 (6) (2021) 1–18.
[3] X.-D. Pan, P.-G. Wu, X.-G. Jiang, Levels and potential health risk of heavy metals in marketed vegetables in Zhejiang, China, Sci. Rep. 6 (1) (2016), https://doi.org/10.1038/srep20317.
[4] S. Praveen, R. Gokulan, T.B. Pushpa, J. Jegan, Techno-economic feasibility of biochar as biosorbent for basic dye sequestration, J. Indian Chem. Soc. 98 (8) (2021) 100107.
[5] I.C. Nwuzor, J.L. Chukwuneke, S.C. Nwanonenyi, I.C. Uche, Comparative Analysis on the Physico-chemical and mechanical properties of agricultural seeds oil modified alkyd resin, Journal of Materials Science Research and Reviews 1 (3) (2018) 1–12.
[6] I.C. Nwuzor, J.L. Chukwuneke, S.C. Nwanoneyi, H.C. Obasi, G.O. Ihekweme, Modification and physiochemical characterization of kaolin clay for adsorption of pollutants from industrial paint effluent, European Journal of Advances in Engineering and Technology 5 (8) (2018) 609–620, 2018.
[7] K.M. Amosa, F.A. Aderibigbe, A.G. Adeniyi, J.O. Ighalo, B.T. Bello, M.S. Jami, M.F.R. Alkhatib, T. Majozi, S.A. Abdulkareem, Auto-correlation robustness of factorial designs and GAMS in studying the effects of process variables in a dual-objective adsorption system, Appl. Water Sci. 11 (2) (2021) 43–57.
[8] J. Wang, S. Wang, Effect of inorganic anions on the performance of advanced oxidation processes for degradation of organic contaminants, Chem. Eng. J. 128392 (2021).
[9] C.A. Igwegbe, O.D. Onukwuli, J.O. Ighalo, C.J. Umembamalu, A.G. Adeniyi, Comparative analysis on the electrochemical reduction of colour, COD and turbidity from municipal solid waste leachate using aluminium, iron and hybrid electrodes, Sustain. Water Resource Management 7 (3) (2021) 39.
[10] M. Bayat, V. Javanbakht, J. Esmaili, Synthesis of zeolite/nickel ferrite/sodium alginate bionanocomposite via a co-precipitation technique for efficient removal of water-soluble methylene blue dye, Int. J. Biol. Macromol. 116 (2018) 607–619.
[11] S. Wang, J. Tian, L. Jia, J. Jia, S. Shan, Q. Wang, F. Cui, Removal of aqueous organic contaminants using submerged ceramic hollow fiber membrane coupled with peroxymonosulfate oxidation: comparison of CuO catalyst dispersed in the feed water and immobilized on the membrane, J. Membr. Sci. 618 (2021) 118707.

[12] D. Sud, G. Mahajan, M. Kaur, Agricultural waste material as potential adsorbent for sequestering heavy metal ions from aqueous solutions – a review, Bioresour. Technol. 99 (14) (2008) 6017–6027, https://doi.org/10.1016/j.biortech.2007.11.

[13] E.C. Chukwuma, J.L. Chukwuneke, J.I. Uba, J.N. Chukwuma, Economic and environmental impact assessment of rainwater harvesting system for a small scale residential area in a typical rural setting, Discovery 59 (2023) e65d1240.

[14] Z. Hao, C. Wang, Z. Yan, H. Jiang, H. Xu, Magnetic particles modification of coconut shell-derived activated carbon and biochar for effective removal of phenol from water, Chemosphere 211 (2018) 962–969.

[15] J.L. Chukwuneke, J.E. Sinebe, H.O. Orugba, H.C. Olisakwe, C. Ajike, Production and physico-chemical characteristics of pyrolyzed bio-oil derived from cow hooves, Arab Journal of Basic and Applied Sciences 29 (1) (2022) 363–371, https://doi.org/10.1080/25765299.2022.2129633.

[16] C.R. Chilakamarry, S. Mahmood, S.N.B.M. Saffe, M.A.B. Arifin, A. Gupta, M.Y. Sikkandar, S.S. Begum, B. Narasaiah, Extraction and application of keratin from natural resources: a review, 3 Biotech 11 (2021) 220.

[17] J.L. Chukwuneke, J.E. Sinebe, H.O. Orugba, C. Ajike, Process optimization for enhancing yield and quality of bio-oil from the pyrolysis of cow hooves, Int. J. Des. Nat. Ecodyn. 17 (3) (2022) 453–461, https://doi.org/10.18280/ijdne.170317.

[18] H. Chen, S. Gao, Y. Li, H.-J. Xu, W. Li, J. Wang, Y. Zhang, Valorization of livestock keratin waste: application in agricultural fields, Int. J. Environ. Res. Publ. Health 19 (2022) 6681.

[19] E. Deydier, R. Guilet, S. Sarda, P. Sharrock, Physical and chemical characterization of crude meat and bone meal combustion residue: waste or raw material? J. Hazard Mater. 121 (1–3) (2005) 141–148.

[20] J.L. Chukwuneke, H.O. Orugba, H.C. Olisakwe, P.O. Chikelu, Pyrolysis of pig-hair in a fixed bed reactor: physico-chemical parameters of bio-oil, South African Journal of Chemical Engineering 38 (2021) 115–120, https://doi.org/10.1016/j.sajce.2021.09.003.

[21] P. Nowicki, I. Kuszyńska, J. Przepiórski, R. Pietrzak, The effect of chemical activation method on properties of activated carbons obtained from pine cones, Cent. Eur. J. Chem. 11 (1) (2012) 78–85, https://doi.org/10.2478/s11532-012-0140-0.

[22] R.R. Karri, J.N. Sahu, Process optimization and adsorption modelling using activated carbon derived from palm oil kernel shell for Zn (II) disposal from the aqueous environment using differential evolution embedded neural network, J. Mol. Liq. 265 (2018) 592–602.

[23] A.E. Ofomaja, E.B. Naidoo, S.J. Modise, Removal of copper(II) from aqueous solution by pine and base modified pine cone powder as biosorbent, J. Hazard Mater. 168 (2–3) (2009) 909–917, https://doi.org/10.1016/j.jhazmat.2009.02.106.

[24] M. Momčilović, M. Purenović, A. Bojić, A. Zarubica, M. Ranđelović, Removal of lead(II) ions from aqueous solutions by adsorption onto pine cone activated carbon, Desalination 276 (1–3) (2011) 53–59.

[25] W. Astuti, R.A. Hermawan, H. Mukti, N.R. Sugiyono, Preparation of activated carbon from mangrove propagule waste by H_3PO_4 activation for Pb^{2+} adsorption, in: AIP Conference Proceedings, vol. 1788, AIP Publishing, 2017, 1.

[26] Arneli, Z.F. Safitri, A.W. Pangestika, F. Fauziah, V.N. Wahyuningrum, Y. Astuti, The influence of activating agents on the performance of rice husk-based carbon for sodium lauryl sulfate and chrome (Cr) metal adsorptions, IOP Conf. Ser. Mater. Sci. Eng. 172 (2017) 012007, https://doi.org/10.1088/1757-899x/172/1/012007.

[27] M. Zięzio, B. Charmas, K. Jedynak, M. Hawryluk, K. Kucio, Preparation and characterization of activated carbons obtained from the waste materials impregnated with phosphoric acid(V), Appl. Nanosci. (2020), https://doi.org/10.1007/s13204-020-01419-6.

[28] S. He, G. Chen, H. Xiao, G. Shi, C. Ruan, Y. Ma, D. Huaming, Y. Bihe, C. Xianfeng, X. Yang, Facile preparation of N-doped activated carbon produced from rice husk for CO2 capture, J. Colloid Interface Sci. 582 (2021) 90–101.

[29] R. Zakaria, N.A. Jamalluddin, M.Z. Abu Bakar, Effect of impregnation ratio and activation temperature on the yield and adsorption performance of mangrove based activated carbon for methylene blue removal, Results in Materials 10 (2021) 100183.

[30] S.C. Iweka, K.C. Owuama, J.L. Chukwuneke, O.A. Falowo, Optimization of biogas yield from anaerobic co-digestion of corn-chaff and cow dung digestate: RSM and python approach, Heliyon 7 (11) (2021) e08255, https://doi.org/10.1016/j.heliyon.2021.e08255.

[31] W.T. Tsai, T.J. Jiang, Mesoporous activated carbon produced from coconut shell using a single-step physical activation process, Biomass Conversion and Biorefinery 8 (2018) 711–718, https://doi.org/10.1007/s13399-017-0288-x.

[32] W.T. Tsai, T.J. Jiang, Y.Q. Lin, Conversion of de-ashed cocoa pod husk into high-surface-area microporous carbon materials by CO_2 physical activation, J. Mater. Cycles Waste Manag. 21 (2019) 308–314, https://doi.org/10.1007/s10163-018-0780-4.

[33] G. Reis, D. Bergna, S. Tuomikoski, A. Grimm, E. Lima, M. Thyrel, N. Skoglund, U. Lassi, S. Larsson, Preparation and characterization of pulp and paper mill sludge-activated biochars using alkaline activation: a box–behnken design approach, ACS Omega 7 (2022) 32620–32630, https://doi.org/10.1021/acsomega.2c04290.

[34] Y.G. Dessie, A.D. Birhan, A. Tsegaye, Optimization of process variables to prepare activated carbon from Noug (Guizotia abyssinica cass.) stalk using response surface methodology, Heliyon 9 (6) (2023) e06626, https://doi.org/10.1016/j.heliyon.2023.e06626.

[35] C.-H. Tsai, W.-T. Tsai, Optimization of physical activation process by CO2 for activated carbon preparation from Honduras mahogany pod husk, Materials 16 (19) (2023) 6558, https://doi.org/10.3390/ma16196558.

[36] A.M. Ghaedi, M. Ghaedi, A.R. Pouranfard, A. Ansari, Z. Avazzadeh, A. Vafaei, I. Tyagi, S. Agarwal, V.K. Gupta, Adsorption of Triamterene on multi-walled and single-walled carbon nanotubes: artificial neural network modeling and genetic algorithm optimization, J. Mol. Liq. 216 (2016) 654–665, https://doi.org/10.1016/j.molliq.2016.01.06.

[37] H.O. Orugba, L.C. Edomwonyi-Otu, Improving the activity and stability of turtle shell-derived catalyst in alcoholysis of degraded vegetable oil: an experimental design approach, Journal of King Saud University-Engineering Science 35 (4) (2021) 297–303, https://doi.org/10.1016/j.jksues.2021.05.001.

[38] H.O. Orugba, C. Osagie, J.E. Sinebe, L.C. Enyi, C.A. Igwegbe, Adsorption of cyanide from Cassava wastewater using activated carbons derived from *Raphia hookeri* kernels: a comparison of *in-situ* and *ex-situ* activation, J. Dispersion Sci. Technol. (2024) 1–12, https://doi.org/10.1080/01932691.2024.2342441.

[39] H.O. Orugba, J.L. Chukwuneke, H.C. Olisakwe, I.E. Digitemie, Multi-parametric optimization of the catalytic pyrolysis of pig hair into bio-oil, Clean Energy 5 (3) (2021) 527–535.

[40] S. Yorgun, D. Yıldız, Preparation and characterization of activated carbons from Paulownia wood by chemical activation with H_3PO_4, J. Taiwan Inst. Chem. Eng. 53 (2015) 122–131.

[41] A. El-Refaey, Comparative performance of cement kiln dust and activated carbon in removal of cadmium from aqueous solutions, Water Sci. Technol.: a journal of the International Association on Water Pollution Research 73 (7) (2016) 1691–1699.

[42] L. Semerjian, Equilibrium and kinetics of cadmium adsorption from aqueous solutions using untreated Pinus halepensis sawdust, J. Hazard Mater. 173 (1–3) (2010) 236–242, https://doi.org/10.1016/j.jhazmat.2009.08.074.

[43] M. Dirbaz, A. Roosta, Adsorption, kinetic and thermodynamic studies for the biosorption of cadmium onto microalgae Parachlorella sp, J. Environ. Chem. Eng. 6 (2018) 2302–2309, https://doi.org/10.1016/J.JECE.2018.03.039.

[44] A.S. Yusuff, L.T. Popoola, E.O. Babatunde, Adsorption of cadmium ion from aqueous solutions by copper-based metal organic framework: equilibrium modeling and kinetic studies, Appl. Water Sci. 9 (4) (2019), https://doi.org/10.1007/s13201-019-0991-z.

[45] J.L. Chukwuneke, M.C. Ewulonu, I.C. Chukwujike, P.C. Okolie, Physico-chemical analysis of pyrolyzed bio-oil from swietenia macrophylla (mahogany) wood, Heliyon 5 (6) (2019) e01790, https://doi.org/10.1016/j.heliyon.2019.e01790.

[46] H.O. Orugba, C. Osagie, D. Ukpenusiowho, C.A. Igwegbe, G.O. Odigie, In-situ and Ex-situ synthesized activated carbons derived from Raphia hookeri Kernels for ibuprofen adsorption in wastewater, Desalination Water Treat. 319 (2024) 100534.

[47] X. Huang, M. Tang, H. Li, L. Wang, S. Lu, Adsorption of multicomponent VOCs on various biomass-derived hierarchical porous carbon: a study on adsorption mechanism and competitive effect, Chemosphere (2022) 137513.

[48] Q. Ji, H. Li, High surface area activated carbon derived from chitin for efficient adsorption of Crystal Violet, Diam. Relat. Mater. 118 (2021) 108516.

[49] W. Wu, S. Bu, L. Bai, Y. Su, Y. Song, H. Sun, G. Zhen, K. Dong, L. Deng, Q. Yuan, C. Jing, Z. Sun, Volatile organic compound removal by post plasma-catalysis over porous TiO2 with enriched oxygen vacancies in a dielectric barrier discharge reactor, Nanoscale (2023), https://doi.org/10.1039/d2nr04952j.

[50] P. Saha, N. Saha, S. Mazumder, M. Reza, Transformation of sulfur during Co-hydrothermal carbonization of coal waste and food waste, Energies 14 (2021) 2271.

[51] V. Volli, A. Gollakota, C. Shu, Comparative studies on thermochemical behavior and kinetics of lignocellulosic biomass residues using TG-FTIR and Py-GC/MS, The Science of the total environment 792 (2021) 148392.
[52] C. Mackie, A. Candian, T. Lee, A. Tielens, Anharmonicity and the IR emission spectrum of neutral interstellar PAH molecules, The journal of physical chemistry A (2022), https://doi.org/10.1021/acs.jpca.2c01849.
[53] Y. Yang, B. Lin, C. Sun, M. Tang, S. Lu, Q. Huang, J. Yan, Facile synthesis of tailored mesopore-enriched hierarchical porous carbon from food waste for rapid removal of aromatic VOCs, Sci. Total Environ. 773 (2021) 145453.
[54] L. Fang, L. Ding, W. Ren, H. Hu, Y. Huang, P. Shao, L. Yang, H. Shi, Z. Ren, K. Han, X. Luo, High exposure effect of the adsorption site significantly enhanced the adsorption capacity and removal rate: a case of adsorption of hexavalent chromium by quaternary ammonium polymers (QAPs), J. Hazard Mater. 416 (2021) 125829.
[55] L. Spessato, V. Duarte, P. Viero, H. Zanella, J. Fonseca, P. Arroyo, V. Almeida, Optimization of Sibipiruna activated carbon preparation by simplex-centroid mixture design for simultaneous adsorption of rhodamine B and metformin, J. Hazard Mater. 411 (2021) 125166.
[56] T.-H. Liou, Development of mesoporous structure and high adsorption capacity of biomass-based activated carbon by phosphoric acid and zinc chloride activation, Chem. Eng. J. 158 (2010) 129–142.
[57] S.S. Lam, R.K. Liew, Y.M. Wong, P.N.Y. Yek, N.L. Ma, C.L. Lee, H.A. Chase, Microwave-assisted pyrolysis with chemical activation, an innovative method to convert orange peel into activated carbon with improved properties as dye adsorbent, J. Clean. Prod. 162 (2017) 1376–1387.
[58] H. Du, J. Cheng, M. Wang, M. Tian, X. Yang, Q. Wang, Red dye extracted sappan wood waste derived activated carbons characterization and dye adsorption properties, Diam. Relat. Mater. 102 (2020) 107646.
[59] V. Chaudhary, K.D. Chaudhary, N. Godara, B. Mordhiya, Study on removal of cadmium (II) ions from wastewater using activated carbon of Salvadora persica stem, Nat. Environ. Pollut. Technol. 13 (3) (2014) 619–622.
[60] A. Jaafar, A. Darchen, S. El Hamzi, Z. Lakbaibi, A. Driouich, A. Boussaoud, A. Yaacoubi, M. El Makhfouk, M. Hachkar, Optimization of cadmium ions biosorption by fish scale from aqueous solutions using factorial design analysis and Monte Carlo simulation studies, J. Environ. Chem. Eng. 9 (1) (2021) 104822.
[61] I. Touzani, I. El Machrafi, K. Harboul, O. Boudouch, I. Alouiz, K. Hammani, R. Flouchi, K. Fikri-Benbrahim, Evaluation of activated carbons prepared from bioprecursors for the removal of cadmium and chromium (VI), Applied and Environmental Soil Science (2024) 8663114.